PAPER

Check for updates

Determination of chloropropanol with an imprinted electrochemical sensor based on multi-walled carbon nanotubes/metal–organic framework composites

Shuang Han, [ID] *[ab] Yuxin Ding,[a] Fu Teng,[a] Aixin Yao[a] and Qiuxue Leng[a]

In this paper, a composite composed of carboxylated multi-wall carbon nanotubes (cMWCNT) incorporated in a metal–organic framework (MOF-199) has been synthesized using 1,3,5-benzoic acid as a ligand through a simple solvothermal method. The synthesized cMWCNT/MOF-199 composite was characterized by scanning electron microscopy (SEM), Fourier transform infrared spectroscopy (FT-IR) and X-ray diffractometry (XRD). The cMWCNT/MOF-199 hybrids were modified on the surface of glassy carbon electrodes (GCE) to prepare a molecularly imprinted electrochemical sensor (MIECS) for specific recognition of 3-chloro-1,2-propanediol (3-MCPD). The electrodes were characterized by differential pulse voltammetry (DPV), electrochemical impedance spectroscopy (EIS) and cyclic voltammetry (CV). Under optimal conditions, the electrochemical sensor exhibited an excellent sensitivity and high selectivity with a good linear response range from 1.0×10^{-9} to 1.0×10^{-5} mol L^{-1} and an estimated detection limit of 4.3×10^{-10} mol L^{-1}. Furthermore, this method has been successfully applied to the detection of 3-MCPD in soy sauce, and the recovery ranged from 96% to 108%, with RSD lower than 5.5% ($n = 3$), showing great potential for the selective analysis of 3-MCPD in foodstuffs.

1. Introduction

3-Chloro-1,2-propanediol (3-MCPD) is categorized as a chlorpropanol, and 3-MCPD in foodstuffs has raised extensive concern in recent years.[1,2] Studies have shown that a long-term intake of 3-MCPD at a low content may lower the sperm count, disturb the balance of sex hormones in the body, and even may be carcinogenic if exceeding certain amounts.[3,4] Recently, some methods have been developed to detect 3-MCPD, such as gas chromatography-mass spectrometry (GC-MS)[5] and gas chromatography (GC). In most studies, due to the low molecular weight of 3-MCPD, the observed limit values are somewhat poor. Moreover these methods require expensive equipment and time-consuming experimental processes.[6]

A molecularly imprinted electrochemical sensor (MIECS) refers to a category of electrochemical sensors that takes molecularly imprinted polymers (MIP) as the sensing element and integrates the molecular imprinting technology and the electrochemical detection. It introduces a novel development and research to analytical chemistry.[7–10] Owing to high specificity for target molecules, remarkable sensitivity, and simple

operation,[11] MIECS have extensive applications in the fields of food security, pesticide residues, environmental detection, clinical medicine and so on.[12–14] To increase the surface area of the modified electrode, materials with excellent performance are usually incorporated.[15] For example, Fang *et al.*[16] prepared MIPs/CDs grafted paper-based sensors to detect 3-MCPD. But due to its paper structure, the mechanical stability of the device is weak. Yuan *et al.*[17] developed a biosensor based on electrocatalytic reduction of hemoglobin (HB) for determination of 3-MCPD. However, the electrochemical sensor is not sensitive because the electroactive center of Hb is deeply buried in the interior.

Metal–organic framework (MOF)[18,19] is a new kind of porous material with three-dimensional network structure, which are formed by self-assembly of metal ions and organic ligands.[20–22] MOF feature large specific surface area and well-ordered pore structure, meriting them extensive applications in such fields as catalysis, sensors, gas isolation and storage.[23] Compared with conventional porous inorganic materials, synthesis conditions of MOF are more moderate and their structures are more viable for modification.[24] Multi-walled carbon nanotubes (MWCNT)[25,26] feature relatively good conductivity and large specific area. They can increase sensitivity for electrochemical sensors and provide more reaction sites for surface of electrodes. The composites made of carbon nanotubes and metal–organic frameworks (MWCNT/MOF) possess such superiorities

[a]College of Chemistry and Chemical Engineering, Qiqihar University, Qiqihar 161006, China. E-mail: iamhanshuang1982@163.com

[b]Heilongjiang Provincial Key Laboratory of Catalytic Synthesis for Fine Chemicals, Qiqihar University, Qiqihar 161006, China
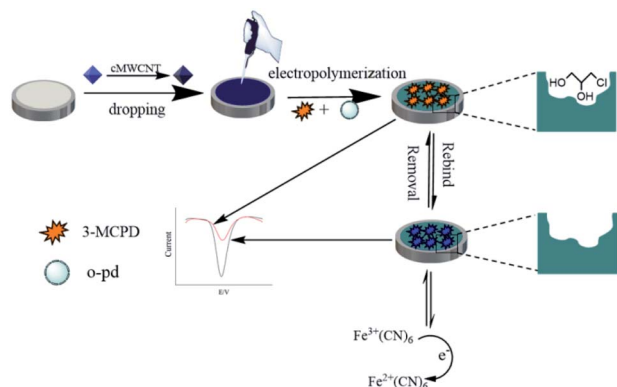
Paper

Fig. 1 Preparation process of MIP/cMWCNT/MOF-199/GCE.

as large specific area, good thermal stability, and extensive pore size distribution. Studies have demonstrated the better performance of MWCNT/MOF hybrid than single materials in the sensors.[27] Recent years, MWCNT/MOF hybrids have attracted much interest in the field of electrochemistry. For example, Guo et al.[28] prepared electrochemical sensors based on MOF/MWCNT, which was applied to the analysis of 4-aminophenol and acetaminophen in Yellow River water and paracetamol tablets. Li et al.[29] developed MOF and MWCNT (ZIF-65@CNTs) by in situ growth of MOF on the surface of carboxylated MWCNT (cMWCNT). By modifying those composites on the surface of glassy carbon electrodes (GCE), they successfully prepared an electrochemical sensor for the detection of ascorbic acid.

In this study, cMWCNT/MOF-199 composites were used as the modified electrodes, potassium ferricyanide as redox probe and a MIECS for specific recognition of 3-MCPD was prepared by electrochemical polymerization using 3-MCPD as the template molecules. The construction principles are shown in Fig. 1. The process could be summarized as follows: (1) the surface of GCE was modified with the cMWCNT/MOF-199 composites to improve the sensitivity and increase the surface area of imprinted platform; (2) electropolymerization of 3-MCPD and o-phenylenediamine (o-pd) on the modified electrode; (3) the template 3-MCPD molecules were removed to form a imprinted sensitive platform as a specific 3-MCPD sensor. The electrochemical sensor showed high sensitivity, good selectivity, stability and repeatability, thus applicable to the detection of 3-MCPD in real samples. This method we proposed provides a new method and a novel idea for the detection of additives in foodstuffs.

2. Experimental

2.1. Materials and reagents

3-MCPD, potassium, o-pd, ferricyanide ($K_3[Fe(CN)_6]$), 1,3,5-benzoic acid (BTC), and $Cu(NO_3)_2 \cdot 3H_2O$ were purchased from Shanghai Aladdin Bio-Chem Technology Co. LTD (Shanghai, China). MWCNT were purchased from J&K Chemical (Beijing, China). N,N-Dimethylformamide (DMF), 1,3-dichloro-2-propanol (1,3-DCP), 2-propanediol and glycerol were purchased from Tianjin Kaitong Chemical Reagent Co. LTD (Tianjin, China).

2.2. Apparatus

All the electrochemical measurements were carried on a CHI 660C electrochemical workstation (CH Instruments, Chenhua Co., China). The X-ray diffraction (XRD) patterns and Fourier-transform IR (FTIR) spectrum were measured with a German Bruker D8-FOCUS X-ray Diffraction and a NEXUS 470 FTIR spectrometer (America).

2.3. Preparation of carboxylated carbon nanotubes

In order to attach negatively charged carboxyl (COOH−) groups on MWCNT sidewalls. Mixed acid liquid-phase oxidation was adopted to prepare functional MWCNT. First, 20 mg of MWCNT was added into 80 mL of HNO_3–H_2SO_4 (v : v = 1 : 3) and reacted at 80 °C for 4 hours. The product was washed with deionized water to pH = 7. The black solid obtained was then placed in an oven at 100 °C for 24 hours, after which cMWCNT were obtained.

2.4. Preparation of MOF-199/cMWCNT composites

MOF-199/cMWCNT composites were prepared by hydrothermal synthesis.[30] First, carboxyl and hydroxyl groups on the cMWCNT surface provide the bonding sites for Cu^{2+} through coordination bonds and hydrogen bonds at the reaction beginning, which further leads to the nucleation and possible priority for MOF-199 crystal growth on the MWCNT surface. For this purpose, 2.0 g of $Cu(NO_3)_2 \cdot 3H_2O$ and 0.2 mg of cMWCNT were dissolved in 17 mL of H_2O by sonication, and the solution was remarked as solution A. Then, 1.0 g of 1,3,5-benzoic acid (BTC) as a ligand was dissolved in 17 mL of N,N-dimethylformamide and 17 mL of ethanol by sonication, and the solution was remarked as solution B. After that, solution A and solution B were mixed and subsequently transferred into a polytetrafluoroethylene kettle for reaction at 120 °C for 24 hours. Here, copper as the central atom, and the oxygen atom in BTC as ligating atom further formed MOF-199/cMWCNT composites. After the reaction, the product was washed three times with DMF and ethanol, and the obtained blue product was placed in an oven and dried at 80 °C for 12 hours.

2.5. Preparation of the modified electrode

The GCE was polished by polishing powder of alumina and rinsed with deionized water. Next, the electrodes were dipped successively in H_2SO_4, anhydrous ethanol and deionized water under sonication for 5 min, after which the electrodes were dried. At last, the bare electrodes were placed in 1 mol L^{-1} H_2SO_4 for activation.

cMWCNT/MOF-199 composites were dissolved in chitosan (CS) solution by sonication. 4 μL of the above solution was dropped on the surface of the GCE. After dried under an infrared lamp, cMWCNT/MOF/GCEs were obtained.

2.6. Preparation of MIP/MOF-199/cMWCNT/GCE composites

First, 3-MCPD (0.5 mmol L^{-1}) as template molecules were interacted with o-pd (3 mmol L^{-1}) as functional monomer

through hydrogen bonding to form pre-polymerization solution. Next, cMWCNT/MOF-199/GCE were placed in this new solution for electro-polymerization, within a potential range of 0–0.8 V. After that, the electrodes were scanned by cyclic voltammetry. On the surface of the modified electrodes, then, molecularly imprinted polymer membranes were prepared. The electrodes were subsequently placed in methanol/acetic acid (v/v = 9 : 1) eluent to remove the template molecules 3-MCPD. At last, the electrodes were taken out, rinsed by distilled water, and dried at room temperature, such that MIP/cMWCNT/MOF/GCE were obtained.

2.7. Detection of real samples

Soy sauce samples were purchased from local supermarkets. Soy sauce samples (1.0 mL) were spiked with a 3-MCPD standard solution at concentration levels of 6.0×10^{-8}, 6.0×10^{-7}, 1.2×10^{-6} mol L^{-1}. After vortex mixing, the samples were centrifuged at 4000 rpm for 10 min at room temperature. The supernatants were ultrasonicated with ethyl acetate (3.0 mL) three times for 15 min each. After keeping steady for 10 min, the resulting extractants were collected, dried under nitrogen flow at room temperature, and then dissolved in 1.0 mL of ethanol solution. The mixture was then centrifuged at 4000 rpm for 10 min, and the clear solution was analyzed using the MIP/cMWCNT/MOF/GCE sensor.

3. Results and discussion

3.1. FT-IR studies

MWCNT, cMWCNT, MOF-199 and cMWCNT/MOF-199 were analyzed by FT-IR spectra. In Fig. 2, the presence of stretching vibration band of –OH at 3440 cm^{-1} of MWCNT is probably due to that the MWCNT absorbed vapors from the air. cMWCNT shows a stretching vibration band of –OH at 3271 cm^{-1}, a stretching vibration band of C=O at 1730 cm^{-1}, a in-plane bending at 1119 cm^{-1}, and a deformation vibration band of –OH at 1045 cm^{-1}, respectively. These suggests the successful

grafting of carboxyl groups onto MWCNT. MOF-199 presents a symmetrical stretching vibration band of H$_2$O absorbed on MOF-199 surface at 3450 cm^{-1}, and symmetrical and asymmetric stretching vibration of –COOH at 1650 cm^{-1}, 1440 cm^{-1} and 1370 cm^{-1}, and no absorption band from 1680 to 1800 cm^{-1}. These indicate complete deprotonation of H$_3$BTC ligands and a complete reaction between H$_3$BTC ligands and Cu^{2+}, from which MOF-199 was generated. Compared with MOF-199, cMWCNT/MOF-199 shows peaks at 2400 cm^{-1} and 2900 cm^{-1} which are associated to hydroxyl groups and stretching vibration band of OH from strongly H-bonded-COOH, respectively. cMWCNT was incorporated in MOF-199 for the presence of some bridge-like bonds or affinity between MOF-199 and cMWCNT,[31–33] such as coordination bonds between metal ions of MOF-199 and carboxyl groups on cMWCNT surface, and hydrogen bonds between carboxyl groups of MOF-199 and carboxyl groups on cMWCNT surface. Thus, the oxygen on the hydroxyl group as the coordination atom provide the lone-pair electrons, resulting in the reduction of the bond force constant and the shift of the absorption frequency to a lower wave number. These suggests the successful bonding between MOF-199 and cMWCNT.[34]

3.2. XRD characterization of MOF-199 and cMWCNT/MOF-199

MOF-199 and cMWCNT/MOF-199 were characterized by XRD, and the results are shown in Fig. 3. Curve a is the spectrum of MOF-199, in which 6.7°, 9.6°, 11.7°, 13.5°, 17.5° and 19.1° are ascribed to the (111), (200), (220), (222), (333) and (440) crystal of MOF-199. The peaks are sharp, indicating the successful preparation and good crystal forms of MOF-199. Curve b shows the XRD spectrum of cMWCNT/MOF-199. Compared with that of MOF-199, cMWCNT/MOF-199 still presents the characteristic peaks of MOF-199. This suggests that the crystal form of MOF-199 was intact after cMWCNT was coated on the surface of it.

3.3. SEM and TEM characterization

The morphology of MOF-199 was characterized by SEM, and the results are shown in Fig. 4a. From the picture, it can be seen
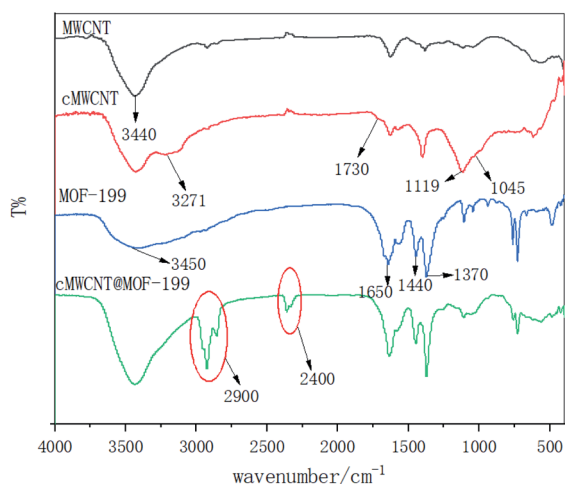

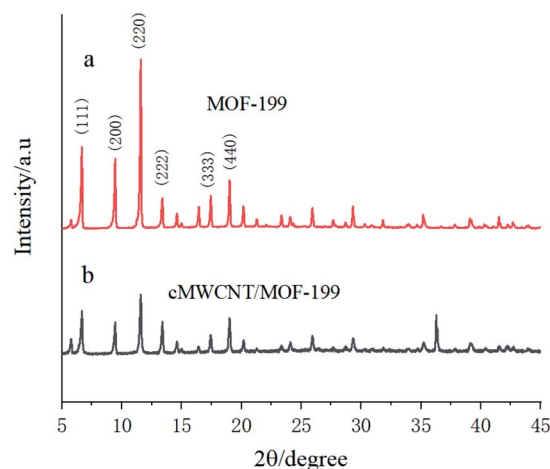Fig. 2 FT-IR spectrums of MWCNT, cMWCNT, MOF-199, and cMWCNT/MOF-199.

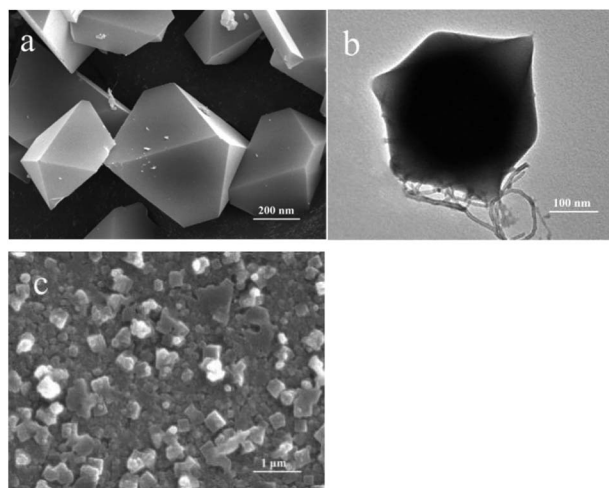Fig. 3 XRD spectrums of MOF-199 (a) and cMWCNT/MOF-199 (b).

Fig. 4 SEM picture of MOF–199 (a), TEM picture of cMWCNT/MOF–199 (b), and SEM picture of MIP/MOF–199/cMWCNT/GCE (c).

that MOF-199 present a regular structure of octahedron, and smooth surface. Fig. 4b re-confirms the implantation of MWCNTs in the MOF-199 matrix which can be clearly seen as transparent tubular structures spread across the octahedral-
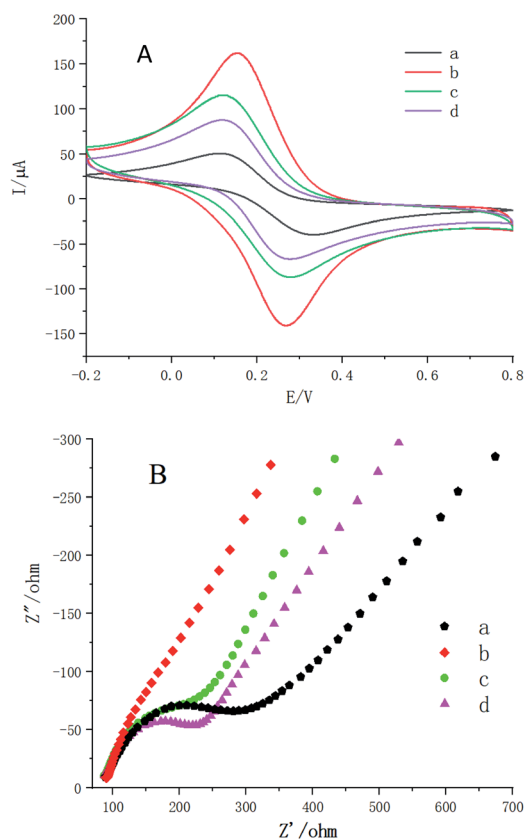

Fig. 5 CV (A) and EIS (B) of different modified electrodes in $K_3Fe(CN)_6$ solution. (Bare electrode (a), cMWCNT/MOF–199 electrode (b), MIP/cMWCNT/MOF–199 electrode (c), and MIP/cMWCNT/MOF–199 electrode after binding template (d)).

shaped crystallites of MOF-199. Fig. 4c shows the morphology of MIP/MOF-199/cMWCNT/GCE, which can be seen that a rough and compact composite covered the electrode surface.

3.4. Electrochemical performances of electrodes

With potassium ferricyanide as redox probe, cyclic voltammetry (CV) and electrochemical impedance spectroscopy (EIS) were applied to characterize the electrodes. The results are shown in Fig. 5. It can be found that the current of cMWCNT/MOF-199 modified electrodes (represented by curve *b*) was apparently higher than that of bare electrodes (represented by curve *a*). This was ascribed to the larger specific surface area and the higher electro-catalytic activity of cMWCNT/MOF-199 to speed up electron transfer. Compared with the modified electrodes (represented by curve *b*), the MIP electrodes (represented by curve *c*) showed a lower current. It was because that though existence of imprinted cavities left by removal of the template molecules, there were non-conductive membranes on the surface of the MIP electrodes, hindering electron transfer. The current of electrode after binding templates (represented by curve *d*) was lower than that of MIP electrodes, (represented by curve *c*) owing to the recombination of the imprinted cavities and the template molecules results in shrinking of conductive area of the electrode. The above results illustrate both the successful preparation of molecularly imprinted membranes and a good electrical conductivity of cMWCNT/MOF-199/GCE.

EIS usually consists of two parts. One of them is a low frequent zone which is under control of diffusion process and often presents as a straight line. The other part is, however, a high frequent zone that is related to the transmission of electrons and often is a semi-circle. The diameter of the high frequent zone corresponds to the resistance of charge transfer
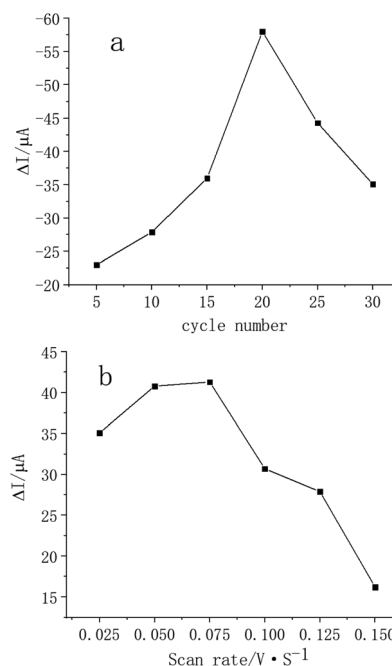

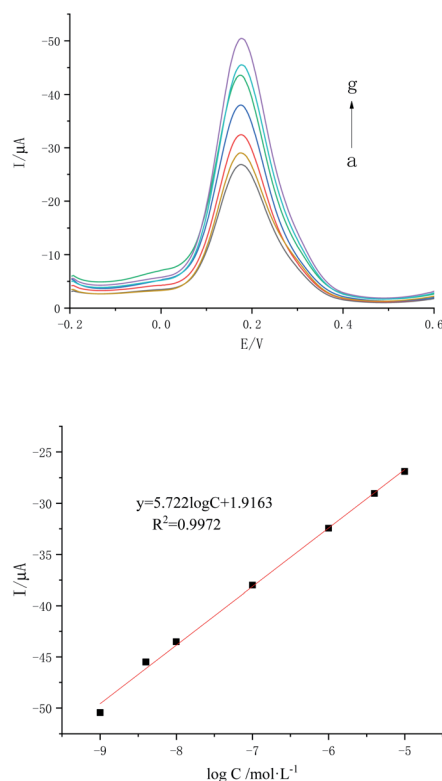**Fig. 6** Optimization of the scan cycles (a) and the scan rate (b).

Fig. 7 Response curve of DPV and linear correction curve (concentrations of 3-MCPD a–g: 1×10^{-5}, 4×10^{-6}, 1×10^{-6}, 1×10^{-7}, 1×10^{-8}, 4×10^{-9}, 1×10^{-9} mol L^{-1}).

Fig. 8 Current response of MIP electrodes to interferents and target.

(R_{ct}) on the surface of electrodes. That is, the larger the diameter, the stronger the resistance, and the lower the corresponding current. The modified electrodes were characterized by AC impedance spectroscopy, as shown in Fig. 5B. The modified electrodes (b) were found having a smaller impedance than the bare electrodes (a). This is due to that the existence of cMWCNT/MOF-199 enlarged surface area of the electrodes and improved the transmission capability of electrons such that the electrical conductivity of modified electrodes increased and impedance decreased. The impedance of MIP electrodes (c) were found larger than that of the modified electrodes (b), which resulted from the increase of impedance because of the existence of non-conductive polymer membranes on their surface. Moreover, the electrodes after binding template (d) showed a larger impedance than the MIP electrodes (c). This was because the imprinted cavities impeded the oxidation–
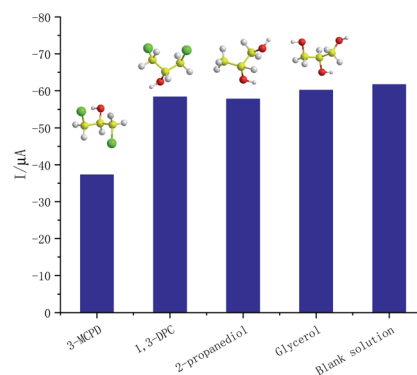
reduction reaction of potassium ferricyanide ions on the surface of the electrodes after absorbing the template molecules, thereby leading to a further increase of the impedance. All the results were coherent with those obtained by the cyclic voltammetry.

3.5. Optimization of preparation conditions for the electrodes

Both the thickness and uniformity of the polymer membrane are critical for the preparation of the electrodes, and they can be affected by the number of polymerization cycles and the scan speed. Insufficient polymerization cycles might lead the imprinted structure easy to be broken while excessive polymerization cycles might lead the template molecules hard to be eluted. Moreover, the scan speed has a direct impact on the uniformity of polymer membrane. Given the background, it is crucial to select an appropriate polymerization cycles and a suitable scan speed. Using differential pulse voltammetry (DPV) method, the effects of scan cycles and the scan rate on the ΔI value of MIP/cMWCNT/MOF/GCE sensor were shown in Fig. 6. It can be seen from Fig. 6 that when the scan cycles are 20, and the scanning speed is 0.075 V s^{-1} the highest ΔI value is obtained.

3.6. Standard curve and detection limit

Under the optimum conditions, DPV was used to detect different concentrations of 3-MCPD. As shown in Fig. 7. It can be found that the electrochemical sensor had a good linear relationship with the current values when the concentration of 3-MCPD in the range of 1.0×10^{-9} to 1.0×10^{-5} mol L^{-1}. The

Table 1 Comparison of the MIP/cMWCNT/MOF-199 sensor with other methods for the quantitative analysis of 3-MCPD[a]

Sensor type	Method	Linear range (mol L^{-1})	LOD (mol L^{-1})	Ref.
MIP-GO/PGE	EIS	2.0×10^{-9} to 5.0×10^{-7}	1.80×10^{-9}	6
MIP/CDs grafted paper	Fluorescence	9.0×10^{-7} to 1.36×10^{-7}	5.40×10^{-9}	16
Hb/MMIPs NPs/GCE	DPV	1.05×10^{-5} to 1.69×10^{-3}	2.60×10^{-7}	17
MIP/cMWCNT/MOF-199/GCE	DPV	1.0×10^{-9} to 1.0×10^{-5}	4.30×10^{-10}	This work

[a] GO: graphene oxide; PGE: pencil graphite electrode; Hb: hemoglobin; CDs: carbon dots.

Table 2 Spiked recovery of 3-MCPD in soy sauce

Samples	Detected	Added/$\times 10^{-8}$ mol L^{-1}	DPV ($n = 3$)			GC-MS ($n = 3$)	
			Found/$\times 10^{-8}$ mol L^{-1}	Recovery/%	RSD/%	Recovery/%	RSD/%
Soy sauce	—	6	6.48	108	2.7	105	5.5
		60	57.6	96	5.5	98	3.1
		120	127.2	106	1.8	104	1.1

equation of linear regression was $y = 5.722 \log C + 1.9163$, with $R^2 = 0.9972$, and the detection limit was 4.3×10^{-10} mol L^{-1} (S/N = 3). Table 1 lists the results of other analytical methods and the quantitative detection of 3-MCPD. The MIP/cMWCNT/MOF-199/GCE sensor was found to have a good linear range, and a lower detection limit.

3.7. Selectivity of MIP/cMWCNT/MOF-199/GCE

To verify the selectivity of the electrodes, MIP/cMWCNT/MOF-199/GCE were placed in 1×10^{-7} mol L^{-1} of 3-MCPD, 1,3-DCP, 1,2-propanediol, glycerol and the control solution, respectively and kept for 10 min. Then the target and interferents in those solutions were detected by DPV. The results are shown in Fig. 8, the prepared electrochemical sensor had a larger current response to 3-MCPD whereas a smaller current response to the analogues. This selectivity might ascribed to the presence of molecularly imprinted membrane which possessed specific recognition sites for 3-MCPD template molecules. The above results demonstrated a good selectivity of the prepared MIP/cMWCNT/MOF-199/GCE to 3-MCPD.

3.8. Stability and reproducibility

To study the reproducibility of MIP/cMWCNT/MOF-199/GCE sensor, five of MIP/cMWCNT/MOF-199 electrodes prepared under the same experimental conditions were used to determine 0.5 mmol L^{-1} of 3-MCPD. The relative standard deviation (RSD) of MIP/cMWCNT/MOF-199/GCE sensor was 3.04%. To

elevate the stability of the sensor, the prepared electrodes were placed in ultrapure water and stored at room temperature for 10 days, with an examination every two days. The RSD of the anodic current detected was 5.61%, showing good reproducibility and stability.

3.9. Application to real sample analysis

The results of spiked recovery experiment on 3-MCPD in soy sauce, are shown in Table 2. The found contents of 3-MCPD in real samples are in good agreement with previous reports.[35] The spiked recovery ranged from 96% to 108%, with RSD < 5.5%. These results demonstrate the proposed method is efficient for accurate determination of 3-MCPD. Moreover, desirable RSD values and recovery percentages are good indicatives for the repeatability and reliability of the proposed method.

As can be seen in Fig. 9, the current response of the spiked samples has almost no change to the standard samples, indicating that the MIP/cMWCNT/MOF-199/GCE sensor has good anti-interference in the detection.

4. Conclusion

In this study, cMWCNT/MOF-199 composites were prepared by combining carbon nanotubes with MOF-199. Furthermore a molecularly imprinted electrochemical sensor capable of specific recognition of 3-MCPD was successfully established by modifying cMWCNT/MOF-199 composites on the surface of GCE. The cMWCNT/MOF-199 composites were found effective in enhancing electrical conductivity, speeding up the transmission of electrons, and improving the sensitivity. The spiked recovery experiment demonstrated that the electrochemical sensor had been successfully applied to the determination of 3-MCPD in real samples, with a detection limit as low as 4.3×10^{-10} mol L^{-1} (S/N = 3). This research provides a new approach and a novel idea for the detection of additives in foodstuffs.

Conflicts of interest

We declare we have no competing interest.
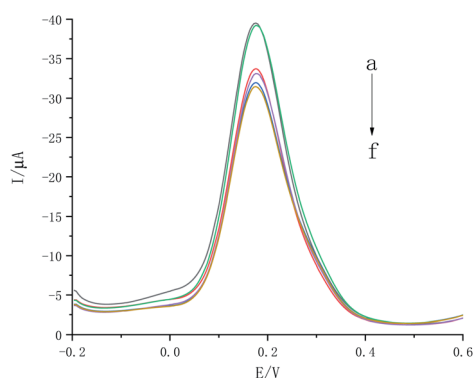
Acknowledgements

Fig. 9 DPV curves of MIP/cMWCNT/MOF-199/GCE electrode in the spiked soy sauce samples and standard 3-MCPD samples ((a, c and e) standard samples with 6×10^{-8}, 6×10^{-7} and 1.2×10^{-6} mol L^{-1} of 3-MCPD, respectively; (b, d and f) spiked real samples with 6×10^{-8}, 6×10^{-7} and 1.2×10^{-6} mol L^{-1} of 3-MCPD, respectively).

References

1 B. S. He, L. Wang and M. N. Li, A biosensor for direct bioelectrocatalysis detection of 3-MCPD in soy sauce using Cyt-c incorporated in Au@AgNSs/FeMOF nanocomposite, *J. Iran. Chem. Soc.*, 2020, **18**(1), 151–158.

2 Q. J. Chai, X. Zhang, E. Karangwa, *et al.*, Direct determination of 3-chloro-1,2-propanediol esters in beef flavoring products by ultra-performance liquid chromatography tandem quadrupole mass spectrometry, *RSC Adv.*, 2016, **13**, 172–184.

3 A. A. Martin, E. K. Fodjo, *et al.*, Simple and rapid detection of free 3-monochloropropane-1,2-diol based on cysteine modified silver nano particles, *Food Chem.*, 2021, **338**, 127787–127793.

4 S. F. Wong, K. H. Low and S. M. Khor, Differential-based biosensor array for fluorescence -chemometric discrimination and the quantification of subtle chloropropanols by cross-reactive serum albumin scaffolding, *Talanta*, 2020, **218**, 121169–121223.

5 S. F. Wong, B. Q. Lee, K. H. Low, *et al.*, Estimation of the dietary intake and risk assessment of food carcinogens (3-MCPD and 1,3-DCP) in soy sauces by Monte Carlo simulation, *Food Chem.*, 2020, **311**, 126033–126040.

6 Y. Y. Tugce, B. Gulcin, S. T. Busra, *et al.*, Molecularly imprinted label-free sensor platform for impedimetric detection of 3-monochloropropane-1,2-diol, *Sens. Actuators, B*, 2021, **328**, 128986–128996.

7 S. Han, F. Teng, Y. Wang, *et al.*, Drug-loaded dual targeting graphene oxide-based molecularly imprinted composite and recognition of carcino-embryonic antigen, *RSC Adv.*, 2020, **10**, 10980–10988.

8 S. Motia, I. A. Tudor, L. M. Popescu, *et al.*, Development of a novel electrochemical sensor based on electropolymerized molecularly imprinted polymer for selective detection of sodium lauryl sulfate in environmental waters and cosmetic products, *J. Electroanal. Chem.*, 2018, **823**, 553–562.

9 S. Han, A. X. Yao and Y. Wang, An ionic liquid–molecularly imprinted composite based on graphene oxide for the specific recognition and extraction of cancer antigen 153, *RSC Adv.*, 2021, **11**(22), 13085–13090.

10 W. Zhang, C. Liu, K. G. Han, *et al.*, A signal on-off ratiometric electrochemical sensor coupled with a molecular imprinted polymer for selective and stable determination of imidacloprid, *Biosens. Bioelectron.*, 2020, **154**, 112091–112100.

11 S. Jafari, M. Dehghani, N. Nasirizadeh, *et al.*, An azithromycin electrochemical sensor based on an aniline MIP film electropolymerized on a gold nano urchins/graphene oxide modified glassy carbon electrode, *J. Electroanal. Chem.*, 2018, **829**, 27–34.

12 J. Shen, T. Gan, Y. S. Jin, *et al.*, Electrochemical sensor based on electropolymerized dopamine molecularly imprinted film for tetrabromobisphenol A, *J. Electroanal. Chem.*, 2018, **826**, 10–15.

13 P. K. Pathak, A. Kumar and B. B. Prasad, Functionalized nitrogen doped graphene quantum dots and bimetallic Au/Ag core-shell decorated imprinted polymer for electrochemical sensing of anticancerous hydroxyurea-ScienceDirect, *Biosens. Bioelectron.*, 2019, **127**, 10–18.

14 Y. F. Sun, H. J. Gao, L. H. Xu, *et al.*, Ultrasensitive determination of sulfathiazole using a molecularly imprinted electrochemical sensor with CuS microflowers as an electron transfer probe and Au@COF for signal amplification, *Food Chem.*, 2020, **332**, 127376–127383.

15 R. Zhao, X. Wu, Y. Gao, *et al.*, A Unique bimetallic MOF derived carbon-MWCNTs hybrid structure for selective electrochemical determination of lead ion in aqueous solution, *Microchem. J.*, 2020, **158**, 105271–105277.

16 M. Fang, L. Zhou, H. Zhang, L. Liu, *et al.*, A molecularly imprinted polymers/carbon dots-grafted paper sensor for 3-monochloropropane-1,2-diol determination, *Food Chem.*, 2019, **274**, 156–161.

17 Y. Yuan, J. X. Wang, X. J. Ni, *et al.*, A biosensor based on hemoglobin immobilized with magnetic molecularly imprinted nanoparticles and modified on a magnetic electrode for direct electrochemical determination of 3-chloro-1, 2-propandiol, *J. Electroanal. Chem.*, 2018, **834**, 233–240.

18 F. H. Wei, Q. H. Ren, H. Zhang, *et al.*, Removal of tetracycline hydrochloride from wastewater by Zr/Fe-MOFs/GO composites, *RSC Adv.*, 2021, **11**, 9977–9984.

19 X. Li, J. Wan, Y. Wang, *et al.*, Mechanism of accurate recognition and catalysis of diethyl phthalate (DEP) in wastewater by novel MIL100 molecularly imprinted materials, *Appl. Catal., B*, 2020, **266**, 118591–118622.

20 R. Fan, N. Kang, Y. Li, *et al.*, A template-directed synthesis of metal–organic framework (MOF-74) ultrathin nanosheets for oxygen reduction electrocatalysis, *RSC Adv.*, 2021, **11**(16), 9353–9360.

21 D. D. Duan, H. Yang, Y. P. Ding, L. Li and G. H. Ma, A three-dimensional conductive molecularly imprinted electrochemical sensor based on MOF derived porous carbon/carbon nanotubes composites and prussian blue nanocubes mediated amplification for chiral analysis of cysteine enantiomers, *Electrochim. Acta*, 2018, **261**, 160–166.

22 N. V. A. Ferraz, W. S. Vasconcelos, C. S. Silva, *et al.*, Gold-copper metal-organic framework nanocomposite as a glassy carbon electrode modifier for the voltammetric detection of glutathione in commercial dietary supplements, *Sens. Actuators, B*, 2020, **307**, 127636–127644.

23 E. Sohouli, M. S. Karimi, E. M. Khosrowshahi, *et al.*, Fabrication of an electrochemical mesalazine sensor based on ZIF-67, *Measurement*, 2020, **165**, 108140–108172.

24 A. Amini, S. Kazemi and V. Safarifard, Metal-organic framework-based nanocomposites for sensing applications, *Polyhedron*, 2019, **177**, 114260–114299.

25 I. ioláková, J. Hovancová, R. Oriňaková, *et al.*, Electrochemical determination of insulin at CuNPs/chitosan-MWCNTs and CoNPs/chitosan-MWCNTs

modified screen printed carbon electrodes, *J. Electroanal. Chem.*, 2020, **860**, 113881–113915.

26 Y. Y. Wu, P. H. Deng, Y. L. Tian, *et al.*, Rapid recognition and determination of tryptophan by carbon nanotubes and molecularly imprinted polymer-modified glassy carbon electrode, *Bioelectrochemistry*, 2020, **131**, 107393–107414.

27 Z. Zhang, Y. Huang, W. Ding, *et al.*, Multilayer Interparticle Linking Hybrid MOF-199 for Noninvasive Enrichment and Analysis of Plant Hormone Ethylene, *Anal. Chem.*, 2014, **86**(7), 3533–3540.

28 H. Guo, T. Fan, W. Yao, *et al.*, Simultaneous determination of 4-aminophenol and acetaminophen based on high electrochemical performance of ZIF-67/MWCNT-COOH/ Nafion composite, *Microchem. J.*, 2020, **158**, 105262–105288.

29 Y. P. Li, W. Ye, Y. J. Cui, *et al.*, A metal-organic frameworks@carbon nanotubes based electrochemical sensor for highly sensitive and selective determination of ascorbic acid, *J. Mol. Struct.*, 2020, **1209**, 127086–127992.

30 H. Y. Zhang, C. Yang, Q. Geng, *et al.*, Adsorption of hydrogen sulfide by amine- functionalized metal organic framework (MOF-199): an experimental and simulation study, *Appl. Surf. Sci.*, 2019, **497**, 143815–143843.

31 X. Wang, N. Yang, Q. Li, *et al.*, Solvothermal synthesis of flower-string-like NiCo-MOF/MWCNT composites as a high-performance supercapacitor electrode material, *J. Solid State Chem.*, 2019, **277**, 575–586.

32 M. Anbia and V. Hoseini, Development of MWCNT@MIL-101 hybrid composite with enhanced adsorption capacity for carbon dioxide, *Chem. Eng. J.*, 2012, **191**, 326–330.

33 D. Micheroni, G. Lan and W. Lin, Efficient electrocatalytic proton reduction with carbon nanotube-supported metal-organic frameworks, *J. Am. Chem. Soc.*, 2018, **140**, 15591–15595.

34 F. Eshraghi, M. Anbia, S. Salehi, *et al.*, Dative post synthetic methods on SBUs of MWCNT@MOFs hybrid composite and its effect on CO_2 uptake properties, *J. Environ. Chem. Eng.*, 2017, **5**(5), 4516–4523.

35 A. E. F. A. Aboelhassan, A. M. I. Gomaa, F. A. NEl-Dien, *et al.*, Validation of an Enhanced Swift Analytical Method for the Determination of Bound and Free 3-chloropropane-1,2-Diol in Foodstuffs using Gas Chromatography–Tandem Mass Spectrometry, *J. Anal. Chem.*, 2020, **75**(11), 1469–1476.